NONLINEAR OPTICS

Linear electromagnetic phenomena are attractive because of their simplicity, elegance, and ease of interpretation. The basic experimental implementation has not changed since the nineteenth century. Although more work continues to be done with increasing sophistication, the applications are identical in their basic form.

Nonlinear optics is useful because of the extreme versatility of the technique. When performing linear optical characterization, the resonance in the material parameters must match the wavelength of the light impinging on the sample. There is no other option. However, in nonlinear optical characterization, there are a large number of possible combinations to make the light waves resonant with the material. Certainly, any of the input waves can be matched to a material parameter. But the difference between input wavelengths can be resonated with a material. Also, the sum of the input waves could provide a resonance. Any imagined combination of frequencies can, under the appropriate circumstances, be used as a means of probing the resonances of a material.

An article of this brevity can by no means contain a complete survey of all techniques for nonlinear optical characterization. As examples of the most visible and most universally applicable techniques, volumes could be written on the subject. There will also be no attempt here to include theoretical derivations of the equations, since excellent discourses are available in the literature (1).

Specifically, this article will discuss stimulated Raman scattering, two-photon absorption, four-wave mixing, high-resolution spectroscopy, detection of rare atoms, multiphoton spectroscopy, and surface nonlinear optical characterization.

STIMULATED RAMAN SCATTERING

Spontaneous Raman scattering is one of the oldest nonlinear optical effects observed. In a vibrational transition that is Raman active, the vibrational excitation contains an anisotropy. This anisotropy allows the vibration to couple to the local electronic excitation. Consequently, when an optical pulse of sufficient intensity travels through a sample, the output will contain frequency sidebands separated from the input frequency by the frequency of the vibrational excitation.

In the stimulated case, the input wave, the material excitation,and the output wave travel as electromagnetically coupled phenomena. Consequently, the signal generated can experience gain analogous to that which occurs in an optical amplifier. Phase-matching considerations force the stimulated Raman scattering (SRS) signal to be generated in a well-defined collimated output. The signal is easier to detect, making it possible to see Raman excitations not seen in the spontaneous case.

The stimulated Raman effect in gases was first reported by Minck, Terhune, and Rado (2). At room temperature, the Q_1 vibrational transition is dominant in the stimulated Raman effect in H_2. A variation in the vibrational frequency with pressure was observed in the spontaneous Raman spectrum. Since the stimulated emission spectrum can display much narrower and more intense lines, this shift was more accurately determined by utilizing Raman laser oscillators. The Stokes and anti-Stokes frequencies (above and below the pump beam) of two H_2 Raman lasers are compared. One laser was operated at a variable frequency and the other has a fixed frequency constant within 0.001 cm^{-1}.

A schematic experimental setup for SRS is shown in Fig. 1 (3). Here the input lasers passes through the sample. PM1 provides calibration, while PM2 measures the forward-gener-

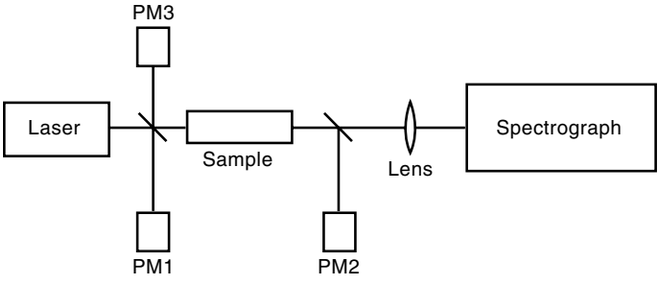

Figure 1. The experimental system for SRS. Although only a schematic, the experimental system here depicts the main elements necessary for performing a measurement of this type. Note that the positioning of PM2 and PM3 permits both forward and backward mesurements to be performed simultaneously. Of importance here is the fact that nothing experimentally exotic is necessary, and the interaction itself provides the information.

ated signal and PM3 measures the backward-generated signal. Data produced from such an experiment are shown in Fig. 2. Although theoretical prediction had shown symmetry in the forward- and backward-generated signals, the data here show a large asymmetry. Work conducted subsequent to this showed that the discrepancy disappeared once self-focusing was taken into account. (These data were performed in liquids that were Kerr active and, consequently, had large degrees of self-focusing.)

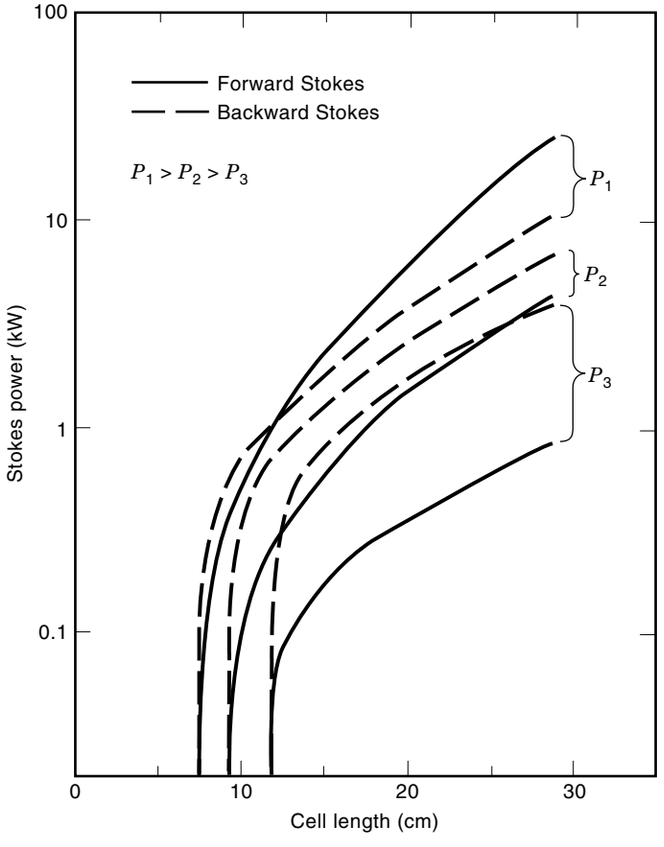

Figure 2. Here is the data collected from each of the detectors shown in Fig. 1. Several important features can be extracted from the data here. There is clearly a threshold intensity needed to initiate the interaction. There is nonlinear dependence of the output power with cell length. Also, the strong asymmetry between the forward and backward signals provides the first indication of the first experimental demonstration of self-focusing, leading to lower thresholds and higher powers in the forward direction.

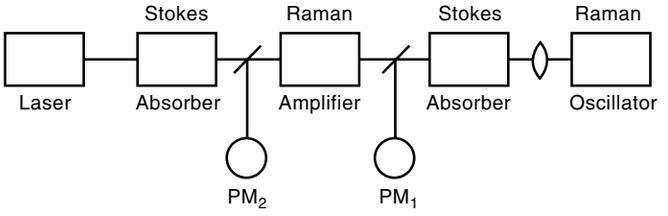

Figure 3. The experimental set-up for the gas phase SRS measurements. Note the relative placement of each of the Stokes and Raman elements, particularly relative to the detector positions.

To eliminate the effect of self-focusing, the experiments can be performed in gas, which does not exhibit self-focusing, as liquids do. Experiments were performed to measure gain at the H_2 vibrational resonance in the forward direction (4). The experimental setup is shown in Fig. 3. The gain of the stable backward amplifier is measured with the setup shown. An important feature is that the geometry of the laser beam in the amplifier cell in both cases is identical to that of the beam emerging from the ruby laser. The laser pulse of about 150 mJ had a 20 ns duration and a diameter of 4 mm. This brings the power flux density to approximately 60 MW/cm^2. Since the geometry of the laser beam is modified in the oscillator cell, this requires the beam splitter arrangement to measure gain in the forward direction.

The experimental gain for the forward and the backward direction as a function of the density is given by the points in Fig. 4. The theoretical curves are included for comparison.

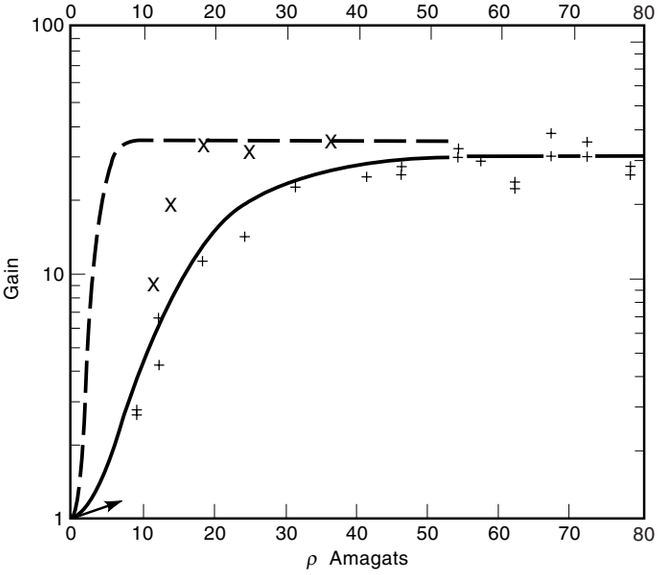

Figure 4. Included with the theoretical curves are the experimental results for forward and backward gain measurements. Since these data were taken in a gas sample, they represented the first measurements devoid of self-focusing. This allowed verification of the SRS theory.

The experimental points X for the forward gain should be compared with the dashed theoretical curve. The experimental points + for the backward gain should be compared with the drawn theoretical curve. Without the effect of self-focusing, there is good agreement between measurement and prediction.

Although it is assumed that nonlinear optical investigations can only be realized with pulsed lasers, it has been demonstrated that SRS can be implemented using continuous-wave (cw) laser sources. This work examines and compares a variety of forms of SRS where cw laser sources may be applied (5). More specifically, direct stimulated Raman gain spectra will be compared with those obtained using optically heterodyned schemes, such as the polarization interference techniques. The use of cw lasers with lock-in detection produces a technique that is extremely sensitive.

Since this work was a demonstration of technique, the experiment was performed on the well-characterized Raman lines in common solvents and mixtures of common solvents. The isotopic mode of benzene at 983.1 cm^{-1} is clearly seen along with the 991.6 cm^{-1} mode of benzene and the 1003 cm^{-1} mode in toluene.

As a demonstration of the sensitivity and resolution of this type of spectroscopy, it was applied to the acquisition high-resolution Raman spectra of a monolayer of chemisorbed *p*-nitrobenzoic acid on aluminum oxide (6). The technique has broad application since it does not require special surface materials or morphology. The spectra are taken in a region near 1610 cm^{-1}, where a strong mode has been observed for *p*-nitrobenzoic acid (PNBA) monolayers in SRS. The technique is introduced as a means of overcoming the sensitivity limitation and luminescence background problems of conventional Raman spectroscopy. A straightforward approach for employing surface picosecond Raman gain (SPRG) is realized for molecular monolayers on dielectric surfaces. In this case, substrate absorption is not important and a simple transmission geometry may be employed. In this article, the measurement explicitly demonstrates the detection of the 1610 cm^{-1} region of the ring quadrant stretch mode of a *p*-nitrobenzoic acid monolayer chemisorbed on an oxidized aluminum surface.

In the experimental setup, two dye lasers are tuned so that their difference frequency coincides with the material excitation at 1610 cm^{-1}. The gain in the anti-Stokes line is monitored as a function of the detuning. The data are shown in Fig. 5. The peaks at 1610, 1600, and 1580 are assigned as Raman peaks since their location did not shift when the stokes laser was shifted by 35 cm^{-1} and repeated spectra were obtained by scanning the pump laser wavelength. The peak at 1610 cm^{-1} is due to the PNBA ring quadrant stretch observed in infrared and enhanced Raman spectra reported previously; the other two peaks are unique to this measurement and seem to imply changes in the condition of the monolayer during the experiments. Evidence suggests that the peaks at 1580 and 1600 are new species formed by photochemical and or thermal reaction induced by the focused beams unique to the measurement.

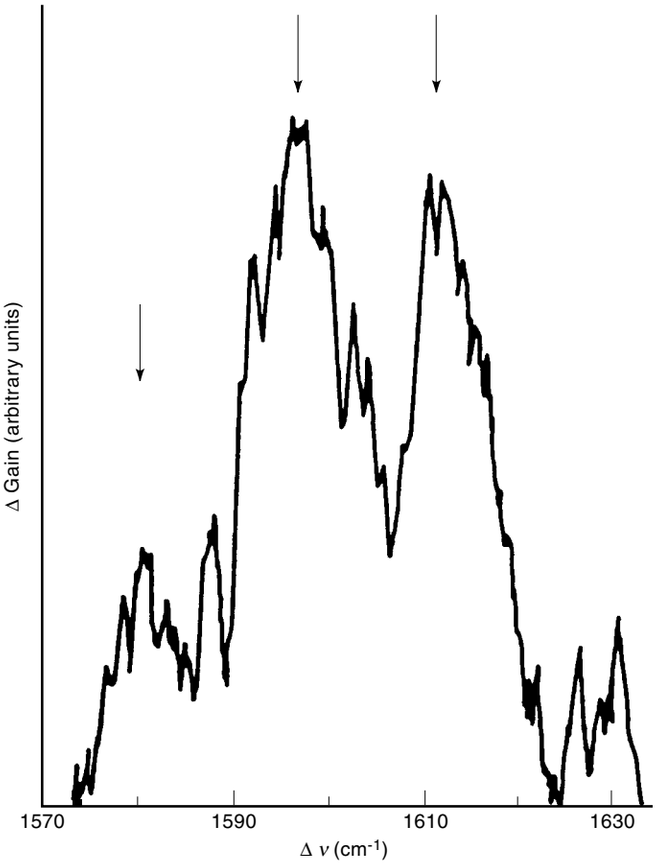

Figure 5. An early optical diagnostic. The existence of three lines in the surface SRS spectra showed that optically induced chemistry could take place at an interface. The data here were anticipated to contain only one peak, so the spectra provided an independent check of their validity.

Stimulated Raman Scattering: Temporal Measurements

Since there are several pulses that enter a sample during SRS, information can be gleaned from an experiment in which one pulse is delayed from the other. This provides a very powerful tool when making temporal measurements on Raman systems. Ordinarily, one would have to measure Raman linewidth and infer the lifetime from the inverse of the bandwidth. A different method for the determination of τ is the use of time-dependent SRS (7). Here, molecular vibrations are coherently excited by a short light pulse and the rise and decay of the vibration amplitude are measured with a second light pulse properly delayed with respect to the first one. For materials with $t > \tau$, that material parameter can be determined. On the other hand, the shape of picosecond light pulses is conserved using samples with $t < \tau$. From this direct measurement, the dephasing time in various materials can be determined.

The experimental system is depicted schematically in Fig. 6. It consists of a modelocked Nd : glass laser that is followed by a single pulse selector. The pulse passes an optical amplifier and a potassium dihydrogen phosphate crystal for conversion to the second harmonic frequency and into the measuring cell. The incident pulse traverses the medium, generating molecular vibration, and Stokes shifts the light. The laser and first Stokes pulses are measured with the fast photocells P1 and P4. The conversion efficiency of a couple percent was kept small to keep the experiment within the range of validity of our theoretical projections. Two beamsplitters provide two

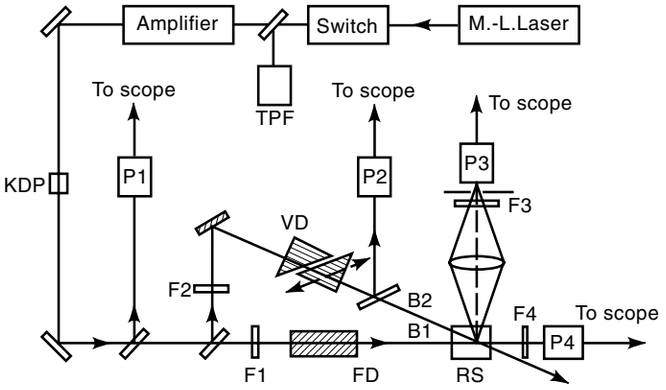

Figure 6. The experimental set-up for time dependent measurements is shown here. The essential element for input is a single short pulse of sufficient energy for the nonlinear interaction to proceed. Then a means of inducing the excitation and measuring its delay is needed. The prism combination is used here for the probe pulse delay.

light pulses of small intensity, approximately 10^{-3} of the pumping pulse. One pulse with variable time delay served as a probe pulse for the vibrational field in the medium, while a second probe pulse with fixed time delay was used as a reference signal to improve the accuracy of our measurements. Both probe pulses are coherently scattered by the molecular vibrations. In this system the anti-Stokes wave generates the phonon and the probe beam interacts with the same phonon to the observed anti-Stokes wave. The system is adjusted for close phase matching with the phonon wave vector collinear with the Stokes and anti-Stokes wave vectors.

The experimental data are shown in Fig. 7. The anti-Stokes line of the probe beam is plotted versus the delay time for carbon tetrachloride and ethyl alcohol. From the data, the material response time τ is measured to be 8.3 ps. Previous

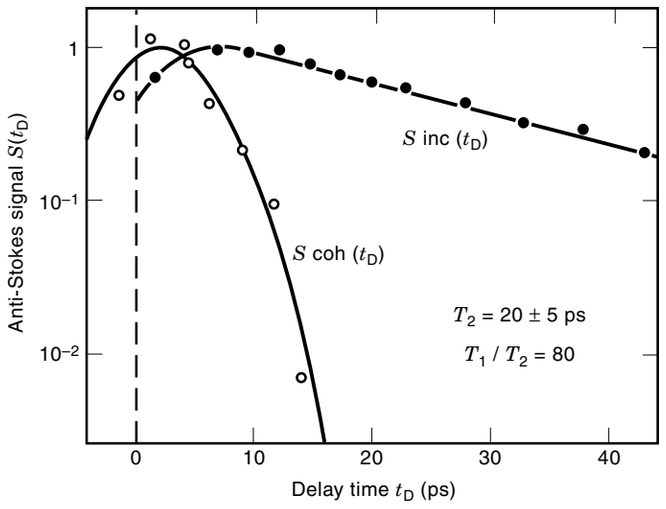

Figure 7. Here are the data from the time delay measurement. For comparison, the open circles show the autocorrelation between pump and probe pulses. The material temporal response is shown in filled circles. Since that decay contains only a single term, the decay is linear on the log scale. Plotting the data on a semi-log scale, as shown, allows one to infer the material dephasing time.

inferences from spectral data gave numbers of 0.26 ps, so the direct measurement is a considerable improvement.

TWO-PHOTON ABSORPTION

The selection rules and, consequently, the spectroscopy of one- and two-photon absorption processes are completely different. This makes them complementary techniques, providing different types of spectroscopic information. In a two-photon absorption process, two photons are simultaneously absorbed with effective photon energy equal to two times the single photon energy. This means that an input laser at frequency ω will be absorbed as if it were light at 2 ω. As a higher-order process, the effective cross section is considerably lower, but with the appropriate choice of intensity, the absorption values can be strong enough to be easily detectable.

One example of this technique is the two-photon absorption measurements performed in single crystal KBr and RbBr (8). The input laser frequency was selected to coincide with the vicinity of the fundamental absorption edge. This electronic absorption is transparent at single photon energy, so that the process has to be two photon in nature. In this experiment a cw source of ultraviolet light is used, which allows a broad spectrum to be evaluated at once. The basic experimental design is shown in Fig. 8. There are several optical filters that have been omitted form the schematic and that are designed to reject stray laser light, which would cause coloration of the sample. To demonstrate that the absorption was actually two photon in nature, the intensity of the laser at the sample was varied. Nonlinear absorption would lead to a decrease in the transmission, which would be proportional to the laser intensity. This was observed. The absorption spectra are show in Fig. 9. Notice that the linear and two-photon absorption spectra are very different in shape. The spectra presented here were sufficiently different that the measurements resulted in a new assignment for the bandgap in the bromide series. This was extremely important because an experimentally determined bandgap is the most important fitting feature in theoretical calculations.

Two-photon spectroscopy can also be performed in gas (9). High-resolution measurements in sodium vapor were performed that were able to eliminate the Doppler background. In this experiment, the sodium atoms are excited to the 4D level by absorbing two photons of 5778 A light, and the resonance is detected by collecting light at the ultraviolet (UV) wavelengths emitted from the 4P level. Important to the application of the technique is that the two-input lasers are counterpropagating beams. Their coincidence in time and space causes the broadening due to the finite velocity of the atoms to be eliminated. The generated spectra clearly show the effect of the hyperfine sublevels in transition between the 3S and 4D states. These lines would be completely obscured by Doppler broadening in a single UV photon absorption measurement.

FOUR-WAVE MIXING SPECTROSCOPY

Technically, this technique is the generalized form of stimulated Raman scattering. The theoretical formalism is the same, only the material resonances do not have to be Raman

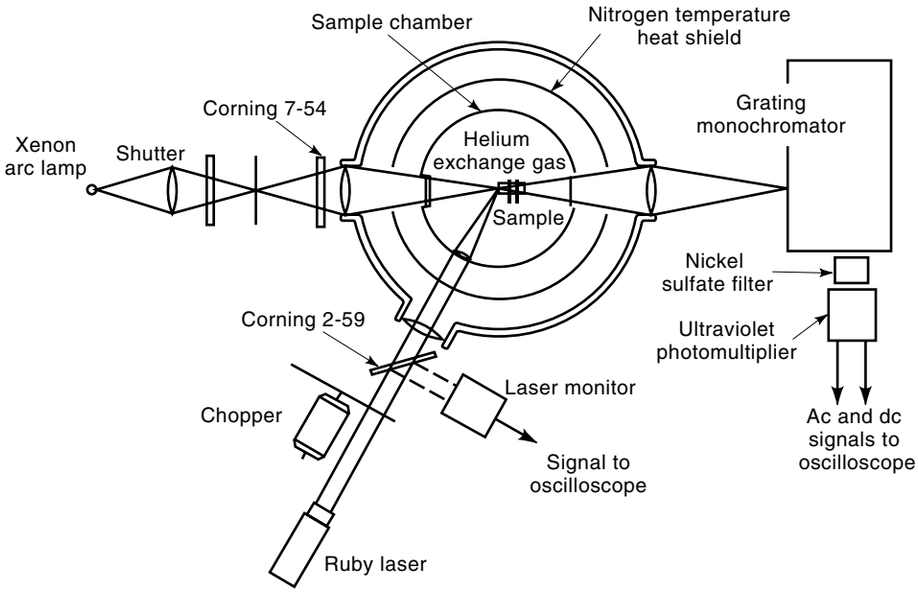

Figure 8. The experimental system demonstrates that two photon mixing need not be derived strictly from a coherent radiation source. In the two photon process, one photon from the ruby laser is mixed with a broadband UV source from a Xenon arc source. The laser energy is near but below the band edge so that a single photon absorption is not possible.

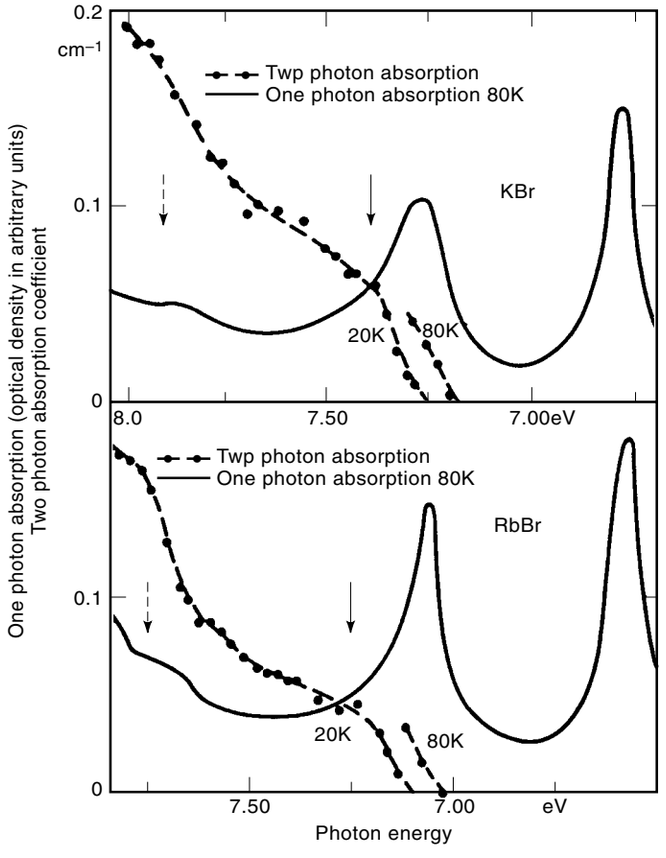

Figure 9. The two-photon and single-photon spectra have selection rules that are very different. The resulting spectra bare little resemblance. The different measurements resulted in a new assignment in the band gap of the bromide series. Linear spectroscopy was sufficiently ambiguous that the assignment would not have been possible without the comparative spectra.

active. Consequently, there will not be gain in the generated signal, but spectroscopic resonances can still be obtained.

One of the most straightforward applications is the so-called induced-grating technique. Two pulses arriving from the same laser that coincide in time but arrive at different angles create an interference pattern on the sample. This pattern will be reflected in the material excitation by producing some photoexcited phenomena with a modulation present on it. A time-delayed third pulse can then be diffracted off the grating. By varying the arrival time of the third pulse and measuring the scattering efficiency as a function of the delay, one can measure the decay time of the excitation in the material.

A typical experimental setup is shown in Fig. 10 (10). The design here is specifically for coherent anti-Stokes Raman spectroscopy (CARS) but is generically equivalent to any four-wave mixing experiment. Two laser inputs have to be provided to the sample. Appropriate control of the inputs and acquisition of the outputs is provided. As the difference between the two input frequencies is made to coincide with a material parameter, the anti-Stokes generated wave will be enhanced.

Experimental measurements are shown in Fig. 11. Here the sample was calcite. The difference between the lasers was tuned to the $1088\,\mathrm{cm}^{-1}$ excitation in calcite. Note that the spectrum is very different from linear spectroscopy. In the linear case, one would see the classical Lorentzian shape. This arises from the imaginary part of the dielectric function in the vicinity of an absorption resonance. However, the presence of a large nonresonant, nonlinear background causes mixing to occur between the real and imaginary components of the dielectric tensor. The resulting spectrum will then become an admixture of the two components.

However, different components of the tensor contribute only to different polarizations in the output signal. A detailed consideration of these contributions enable one to select which parts of the dielectric function will dominate the output spectrum (11). Results from this type of experiments are

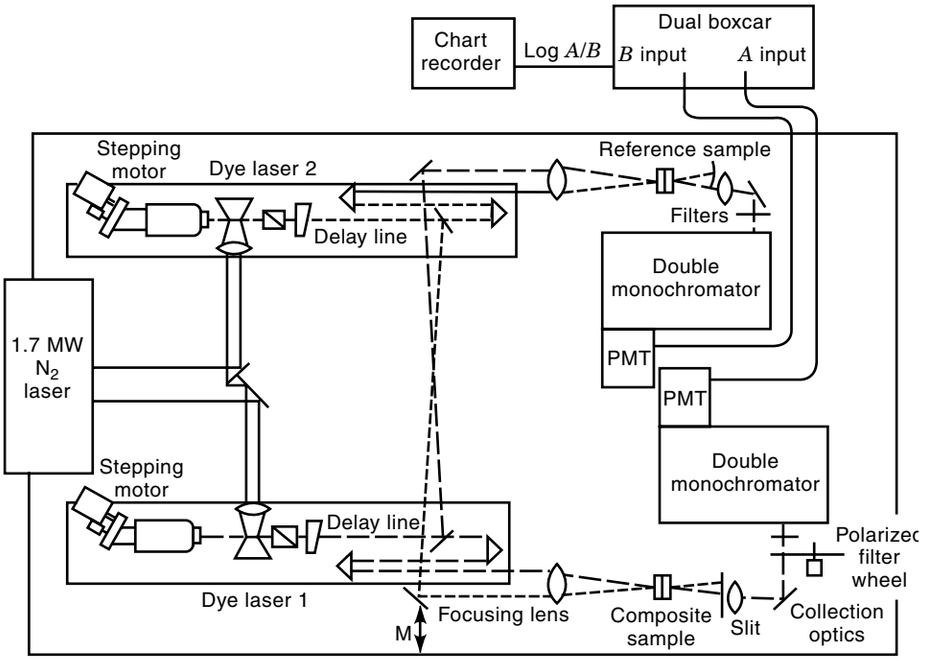

Figure 10. The experimental schematic contains all the basic features necessary for a four wave mixing experiment. Although it is not necessary to have a single pump for the two lasers, a means of synchronizing the inputs is still required. Beyond that, careful references are needed to null any fluctuations, since the nonlinearity of the response could be completely washed out otherwise.

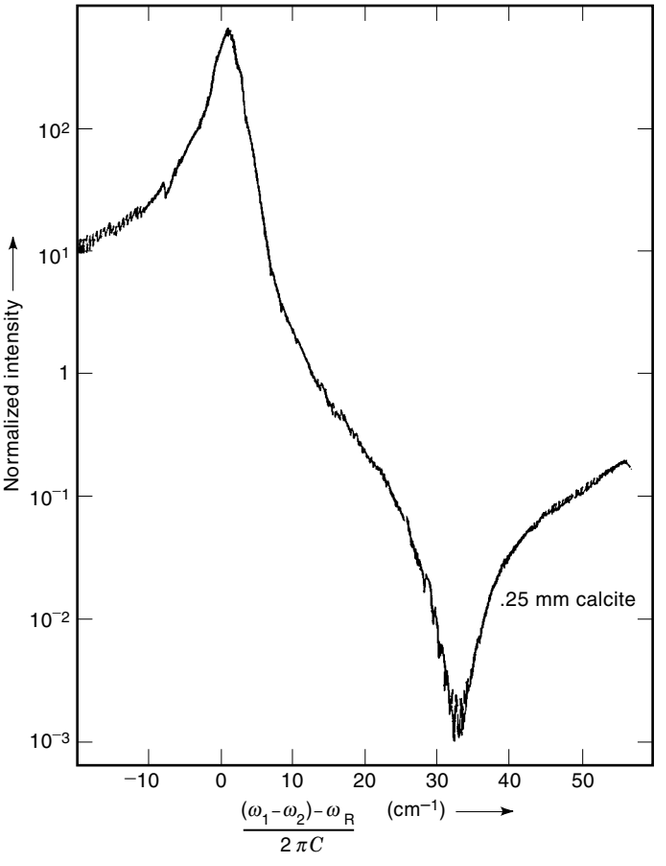

Figure 11. A typical four wave mixing resonance contains not just the peak when the frequency mixing is on resonance with the material excitation. There will also be a dip below the nonresonant background due to the interference between the real and imaginary parts of the dielectric function.

shown in Fig. 12. Here the sample is dilute mixtures of benzene in carbon tetrachloride. By varying the appropriate polarization component of the anti-Stokes output, the desired spectral features can be ascertained as shown in the data. Graph (a) demonstrates how the choice of polarization can eliminate the nonresonant background. Graphs (b) and (c) show how the imaginary or real part of the dielectric function can be brought out from the sample.

HIGH-RESOLUTION NONLINEAR SPECTROSCOPY

Although lasers themselves have linewidths that are intrinsically narrow, most spectroscopic lines in nature are inhomogeneously broadened. Consequently, the fine (narrow) features wash out when using standard linear absorption techniques. As an example, the Doppler width of the sodium D lines are over 1 GHz, while the hyperfine splittings are sub-GHz. Nonlinear optical spectroscopic techniques provide several means that reduce the effects of the inhomogeneous broadening in a sample. Several examples of these techniques are discussed here.

As an example, high-resolution nonlinear optics was performed using quantum beats in Cs vapor (12). If an atom is prepared in a coherent superposition of states by a pulse excitation, modulations in the fluorescence signal at frequencies corresponding to the energy splittings may be observed. By carefully optimizing the experimental procedures, the optically excited hyperfine splittings were able to be observed. This was difficult because the small splittings result in very fast modulations that are difficult to observe. Specifically, the light emitted by the $7^2P_{3/2}$ level of Cs^{133} was observed after excitation by a short laser pulse. The energy-level diagram of Cs with the hyperfine splittings is shown in Fig. 13.

The physical process is quantum mechanical in origin. Once the excitation process by laser absorption occurs, the hyperfine coherence starts evolving at different eigenfrequencies that correspond to the energy splittings between the ex-

cited levels. Since the fluorescence from these levels depends on the state at the time of emission, the intensity of the fluorescence light must exhibit the same temporal behavior as the temporal behavior of the atoms.

In the experimental setup, a 2 ns pulse of 1 GHz bandwidth impinges on the sample. The fluorescence signal is monitored by repetitive measurement of the fluorescence. (At the time this work was conducted, real-time signal processing did not exist and the signal temporal shape had to be measured by sampling. This would not be necessary with present technology.) Figure 14 shows the beat signals corresponding to the resonances in the Cs. The theoretical plots are shown below each picture. As can be seen, the predicted behavior matches the measured signal to a high degree of precision.

Performing a Fourier transform on the signal, one finds the three peaks at the frequencies corresponding to each beat signal. The transform is shown at the bottom of Fig. 14.

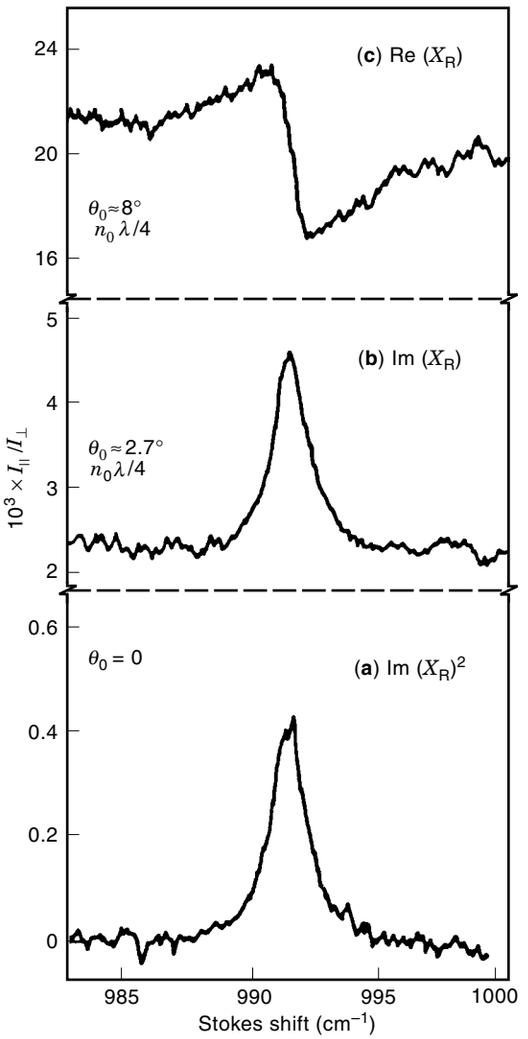

Figure 12. Using the polarization properties of four wave mixing, the signal can be changed to emphasize the real or imaginary parts of the signal. Part (a) of the figure is the magnitude of the Stokes resonance, but (b) and (c) contain dominantly imaginary and real parts, respectively.

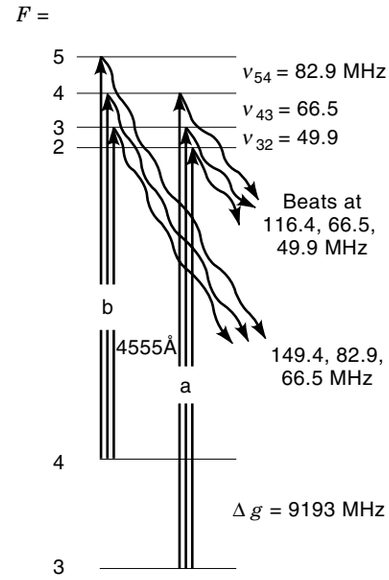

Figure 13. The theoretical energy level diagram shows the multitude of hyperfine structure lines which exist within the Doppler broadened resonance.

Another example is the so-called Doppler free spectroscopy (13). Doppler broadening is caused by the large range of velocities within an atomic sample. Cooling the sample can narrow the spectrum, but only by a limited amount. A more effective means would be to create a situation in which only a limited velocity span could interact with the atoms. In Doppler free spectroscopy, two counterpropagating lasers interact with a sodium beam.

The experimental setup is shown in Fig. 15. Here, the counterpropagating lasers are generated by retroreflecting the input laser. As a two-photon absorption, the laser frequency is tuned to half the absorption frequency. Since the absorption is weak, the return beam is almost the same strength as the input beam. This simple scheme allows quick resolution of the hyperfine levels in Na, as shown at the bottom of the figure.

DETECTION OF RARE ATOMS AND MOLECULES

A specialized but important application nonlinear optics is in the detection of a small number of atoms and molecules. Florescence techniques are known to be very sensitive due to the optical labeling of certain species. Careful optimization of the experimental apparatus can make it possible to detect single atoms. An example is presented here.

Resonance fluorescence can detect the presence of a small amount of atoms because of the relatively large number of photons per second that can be scattered from the atoms in question (14). The first step here is the use of fluorescence to make absolute measurements of sodium vapor densities.

The experimental apparatus is shown in Fig. 16. A laser input is tuned to one of the resonant sodium lines. The florescence is collected in sidelight and analyzed. The sodium oven temperature is varied as a means of controlling the density of vapor in the cell. Phase-sensitive (lock-in) electronics

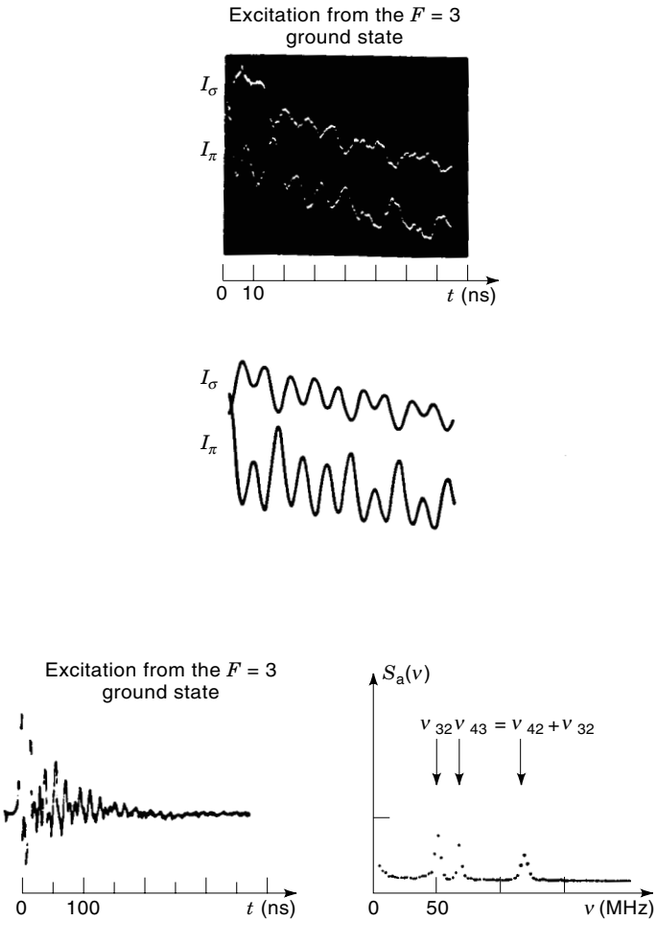

Figure 14. Observing the beat frequencies from the time dependent output spectra, one can see the interference in the terms of the signal. Fourier analysis of the signal shows the multiple components that are present. Their frequency and relative strength can be determined to a high degree of resolution and accuracy.

enables detection sensitivity to less than 100 atoms per cubic centimeter.

The results of these measurements are shown in Fig. 17. As can be seen, the measurements cover many orders of magnitude, from 10^2 atoms/cm^3 to 10^{11} atoms/cm^3. Furthermore, coupling the spectroscopy data with thermodynamic measurements allows the curve to be absolutely calibrated without any variable parameters in the fit to the theoretical curve (solid line).

MULTIPHOTON SPECTROSCOPY

One of the most exciting and surprising techniques in nonlinear optical characterization is multiphoton spectroscopy. Not only can one access states that cannot be probed by single-photon methods, but transitions between excited states can be examined as well. One can think of multiphoton spectroscopy as a generalization of the two-photon and stimulated Raman spectroscopies discussed in this article. The formalism remains the same, but the applications here are more exotic.

In one experiment, multiple-photon excitation was used to prepare Sr in autoionizing Rydberg states (15). Separate excitations were used in this case. The process excited the first electron to a Rydberg state and then the excitation of the remaining 5s core electrons to the $5p_{1/2}$nd state. This produces large amounts of population in the latter state,which is autoionizing and can therefore be detected with nearly unit efficiency. Because the stepwise excitations are all dipole allowed, the required laser powers are low, resulting in no background because of photoionization. Using two synchronous pumped lasers at 460 m and 4194 nm, Sr molecules in an atomic beam are excited to the $5S_2$ states, to the 5s, 5p, and to the 5s, 20s bound Rydberg state. After excitation to this state, a laser at 4218 nm excites the remaining 5s core electron, producing an autoionizing state. A small electric field is applied, and this sweeps the electron out of the $5p_{1/2}$20s state, which is counted. By measuring the electron's number as a function of the third laser pulse, the spectra of the $5p_{1/2}$,nd state and $5p_{1/2}$,ns states can be attained. The spectra obtained are shown in Fig. 18. In these spectra, the quantum defect is strongly represented. The upper curve shows two peaks because of the strong coupling to the defect. The lower curve has only a single peak due to its relatively weak coupling.

Another example is the use of multiphoton excitation of Na to study the diamagnetic structure of Na Rydberg states (16). The goal in this experiment was to study the one-electron atom in a field so intense that the Lorentz force on the electron dominates the Coulomb interaction. Although the field required cannot be achieved in the laboratory, the experimental measurements approaching the strength would help to explain some of the interactions that are not well understood.

In the experiment shown in Fig. 19, an atomic beam is excited to a Rydberg state by a two-photon excitation. After this, an electric field is applied to ionize the Rydberg state and collected. The experiment then measured the collected energy as a function of applied magnetic field. The results are shown in Fig. 20. The solid lines represent the calculated shifts in each of the Rydberg states as a function of magnetic field. This shows very good agreement. Note that the use of the Rydberg state, not possible without the multiphoton excitation, makes it possible to create an atom that can be well characterized by a single electron model, so that it is possible to eliminate the multibody interaction and concentrate on the interaction with the magnetic field.

SURFACE NONLINEAR OPTICAL CHARACTERIZATION

One of the most recent applications of nonlinear optics to characterization is the use of second-order nonlinear optics to study surfaces and interfaces. It is well known that symmetry considerations prevent second-order nonlinear optical processes from proceeding in centrosymmetric media. (To be completely precise, this is only the case in the electric dipole approximation. However, the magnetic dipole and electric quadrupole contributions are so weak that they are usually ignored on the surface.) Since the symmetry is broken at a surface or interface, second-order nonlinear optical processes become surface specific. Consequently, a whole host of surface physics and chemistry problems, which previously could only be performed in ultra-high vacuum (UHV), now become trac-

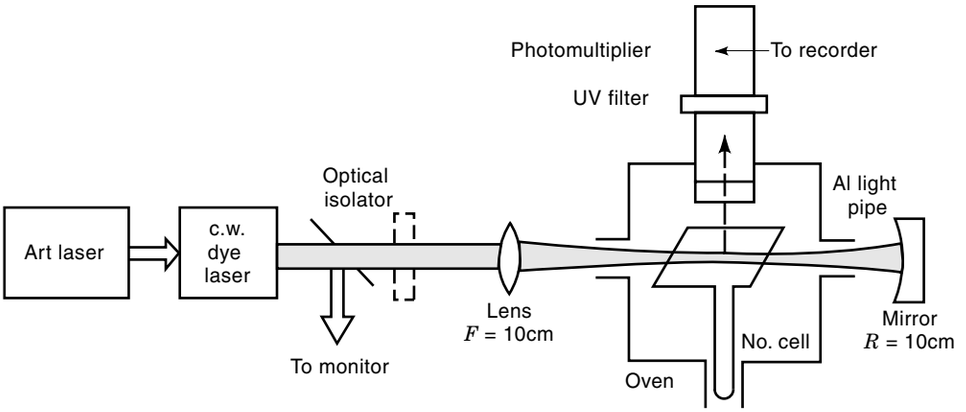

(**a**)

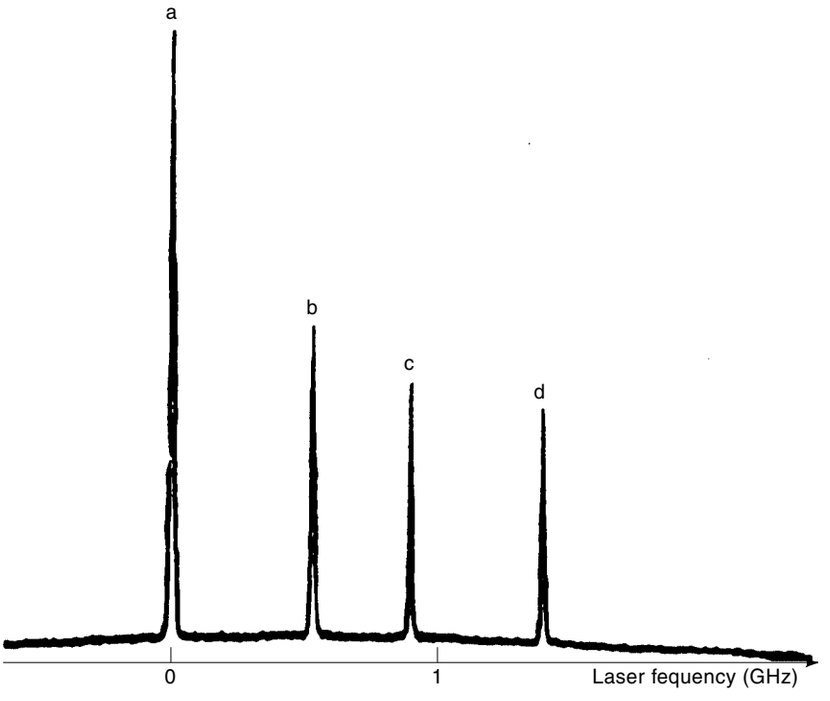

(**b**)

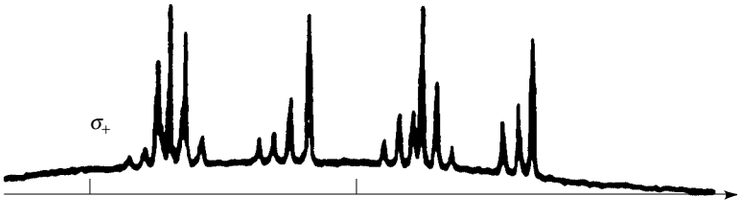

(**c**)

Figure 15. The upper half (a) of the figure shows the preparation of the sodium cell and the manner in which the saturation configuration is effected. Note that there is not a separate return beam. The retroreflection acts as its own second pass. The extremely narrow linewidths resulting from the Doppler free signal are shown in (b) and (c).

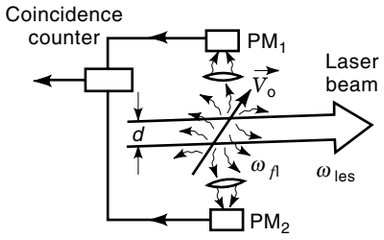

Figure 16. The schematic representation is shown to illustrate how the coincidence counts from the fluorescence signal are created and detected.

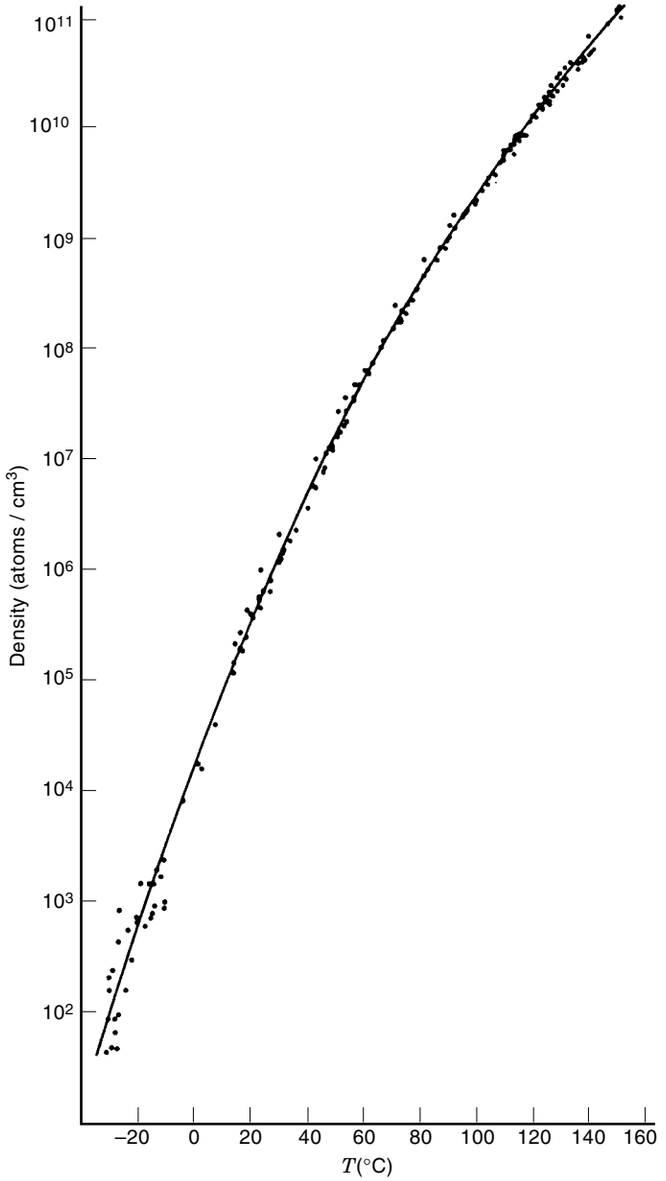

Figure 17. The fluorescence signal from the rare atom detection. Note that the signal can detect the presence of fewer than 100 atoms per cubic centimer. Additionally, the signal range extends over 9 orders of magnitude, an extremely large range over which to produce data.

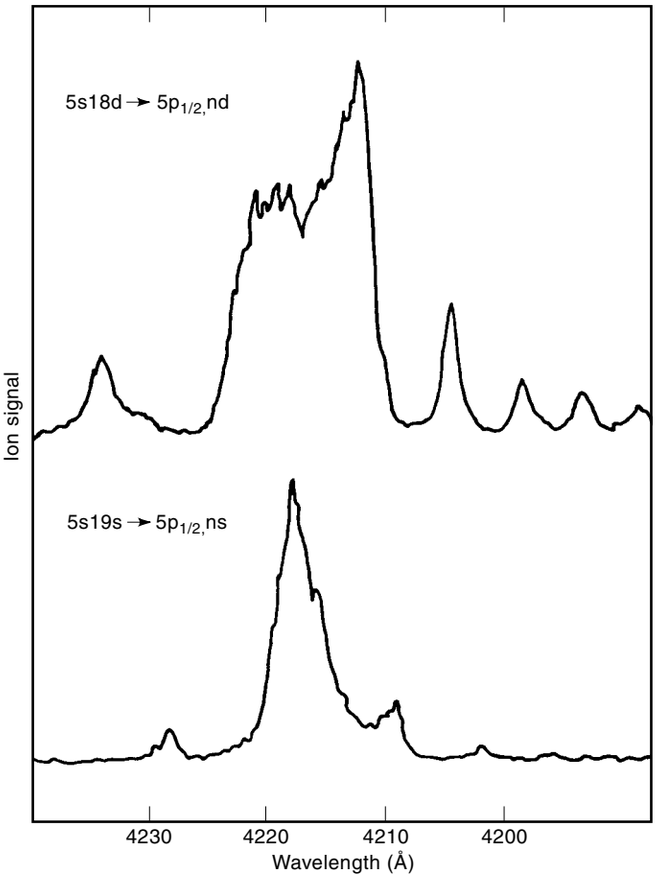

Figure 18. The Rydberg spectroscopy allowed the first observation of quantum mechanical effects in high lying energy states. The strong defect coupling distorts the upper curve while not affecting the lower one. It is not possible to determine this type of interaction by other means.

table experimental problems. Presented here are the experimental techniques and some examples of the sorts of measurements that can be performed.

The experimental setup for second harmonic generation is quite simple. The input laser is focused to the desired spot

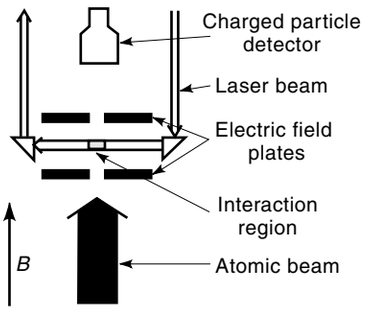

Figure 19. The experimental configuration for the high magnetic field strength spectroscopy. The particular configuration is such that the atomic beam magnetic field and electric field (for ionization) are all collinear, while the laser propagates in a plane normal to that axis.

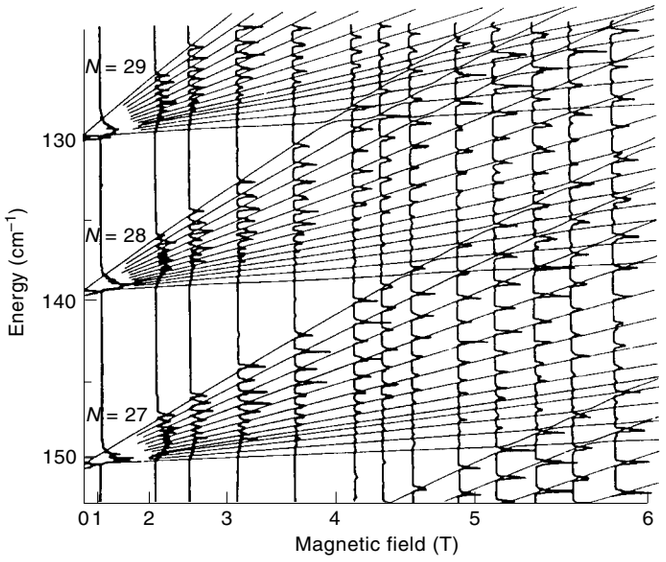

Figure 20. The spectroscopy of the high N states in the Rydberg atom shows the strong effect that the magnetic field can have on the spectroscopy. Note that the field predominates at 4 to 5 T such that the states of differing N begin to overlap. The theory does, however, still provide good agreement with experiment in spite of the large shifts.

size on a surface or interface. Due to the surface phase-matching constraints, the second harmonic generated at the surface will propagate in the same direction as the reflected fundamental. Optical filtering is necessary to eliminate the fundamental, but the second harmonic signal is strong enough to detect with standard detection schemes.

An example spectroscopic sample is shown in Fig. 21 (17). The two rhodamine molecules have excitations that are near each other but do not exactly coincide. The shift is due to the slight difference in their molecular structures as shown. After preparing two samples of glass substrates with molecular coatings, the second harmonic spectra is as shown in Fig. 22. A slight shift is seen between the two samples. Note that these signals, with excellent signal to background, are generated from single molecular monolayers.

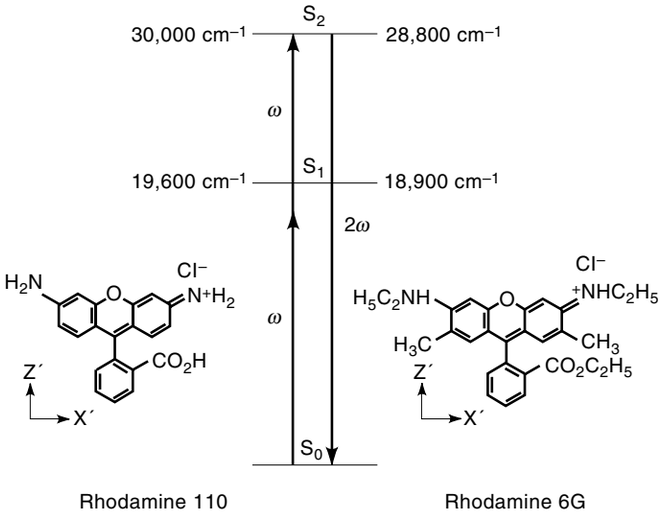

Figure 21. The second harmonic excitation spectra of the rhodamine 110 and 6G molecules differ slightly in the position of their resonant peaks. The slight change in the molecular structure, as shown, causes the shift.

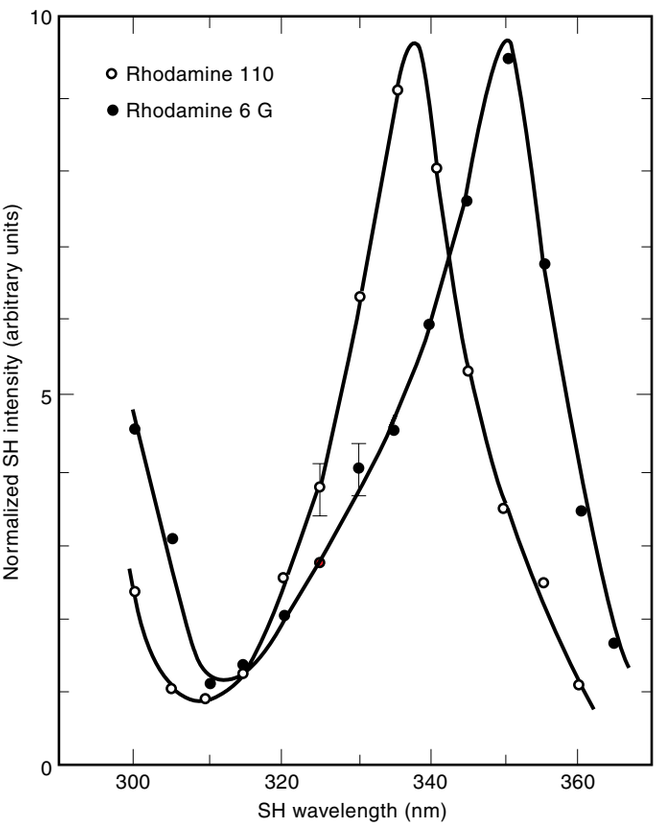

Figure 22. The surface second harmonic spectra of a molecular monolayer of the dye molecule adsorbed to a glass substrate. This represents one of the first examples of the use of second-order nonlinear optics as a means for providing surface sensitive optical characterization. This demonstrates the potential for performing surface species identification in an in-situ fashion. Odd order optical techniques could also access this information, but they would have large contributions from the bulk substrate.

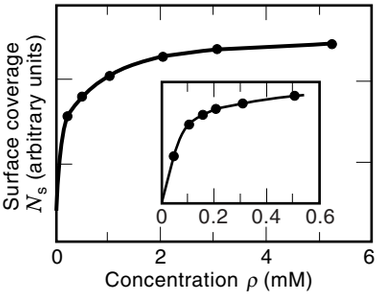

Figure 23. Other than surface second-order nonlinear optics, there is no manner in which to perform surface sensitive spectroscopy at a solid liquid interface. The measurement demonstrates how the surface molecular adsorption from solution can be measured in-situ.

The technique can also be used as an in situ probe of effects at a solid liquid interface. Figure 23 shows the second harmonic strength of a signal generated at a glass ethanol interface as a function of *p*-nitrobenzoic acid concentration (18). As the PNBA adsorbs to the glass, the surface coverage increase and the resulting second harmonic signal increases. There is no other technique that can monitor, to this level of sensitivity, a chemical process at a liquid/solid interface.

BIBLIOGRAPHY

1. Y. R. Shen, *The Principles of Nonlinear Optics,* New York: Wiley, 1984.
2. R. W. Minck, R. W. Terhune, and W. G. Rado, Laser-stimulated Raman effect and resonant four-photon interactions in gases H_2, D_2, and CH_4, *Appl. Phys. Lett.,* **3**: 181–184, 1963.
3. Y. R. Shen and Y. J. Shaham, Self-focusing and stimulated Raman and Brillouin scattering in liquids, *Phys. Rev.,* **163**: 224–231, 1967.
4. N. Bloembergen et al., *IEEE J. Quant. Elect.,* **QE-3**: 197, 1967.
5. A. Owyoung, *IEEE J. Quant. Electr.,* **QE-14**: 192, 1978.
6. J. Heritage and D. L. Allara, *Chem. Phys. Lett.,* **74**: 507, 1980.
7. D. Von der Linde, A. Laubereau, and W. Kaiser, *Phys. Rev. Lett.,* **26**: 954, 1971.
8. D. Frolich and B. Staginnus, *Phys. Rev. Lett.,* **19**: 496, 1967.
9. J. J. Hopfield, J. M. Worlock, and K. J. Park, *Phys. Rev. Lett.,* **11**: 414, 1963.
10. M. D. Levenson, *IEEE J. Quant. Electr.,* **QE-10**: 110, 1974.
11. J-L. Oudar, R. W. Smith, and Y. R. Shen, *Appl. Phys. Lett.,* **34**: 758, 1979.
12. S. Haroche, J. A. Paisner, and A. L. Schawlow, *Phys. Rev. Lett.,* **30**: 948, 1973.
13. T. W. Hansch, in N. Bloembergen (ed.), *Nonlinear Spectroscopy,* New York: North-Holland, 1977, p. 17.
14. W. M. Fairbank, T. W. Hansch, and A. L. Schawlow, *J. Opt. Soc. Am.,* **65**: 199, 1975.
15. W. E. Cooke et al., *Phys. Rev. Lett.,* **40**: 178, 1978.
16. M. L. Zimmerman, J. C. Castro, and D. Kleppner, *Phys. Rev. Lett.,* **40**: 1083, 1978.
17. T. F. Heinz et al., Spectroscopy of molecular monolayers by resonant second-harmonic generation, *Phys. Rev. Lett.,* **48**: 478–481, 1982.
18. T. F. Heinz, H. W. K. Tom, and Y. R. Shen, Detection of molecular orientation of monolayer adsorbates by optical second-harmonic generation, *Phys. Rev.,* **A28**: 1883–1885, 1983.

JEFFREY H. HUNT
Boeing North American

NONLINEAR OSCILLATORS. See RELAXATION OSCILLATORS AND NETWORKS.

NONLINEAR POLYNOMIAL EQUATIONS. See POLYNOMIALS.